Chemistry—Methods

Research Article
doi.org/10.1002/cmtd.202500102

Chemistry Europe
European Chemical Societies Publishing

www.chemistrymethods.org

Following Changes at the Solid/Liquid Interface for Large Microplastic Particles by Streaming Potential

Matthias B. Engelhardt, Daniel Wagner, Mohsen Zarebanadkouki, Nora Meides, Christian Schulbert, Martin G. J. Löder, Nicolas Helfricht, Seema Agarwal, Andrea Carminati, Peter Strohriegl, Jürgen Senker, Christian Laforsch, and Georg Papastavrou*

The electrolyte/solid interface is ubiquitous in nature and for many applications. In particular, the double-layer properties are essential for predicting adsorption and transport behavior. While for small colloidal particles, electrophoretic mobility has developed into a routine technique, there is currently a lack of analogously established techniques for particles with diameters larger than 10 microns. Such particles are often encountered in natural soils, industrial formulations, and as contaminants in the form of microplastics. Herein, a systematic method development using the streaming potential technique of particle plugs composed of large particles is presented. This approach revives an analytical method that was first introduced nearly 75 years ago, which has rarely been used for particulate systems. Comparing the zeta-potential versus pH of polystyrene particles with varying surface functionalization demonstrated that streaming potential measurements can distinguish these surface groups. In agreement with theoretical predictions, no dependence on the particle dimensions and shape is observed. Moreover, the particle arrangement within the particle plugs has been characterized by X-ray microtomography. The viability of this technique is tested by monitoring the artificial weathering of artificially fragmented microplastic particles of nonspherical shape. This technique opens new possibilities for characterizing the interfacial properties of environmentally relevant microplastics.

1. Introduction

Microplastic particles (MPP) are among the most widespread environmental contaminants.[1–7] They can be found in aquatic and terrestrial environments, including rivers, soil, and the sea; MPPs are also present geographically everywhere on earth, even in remote locations such as Antarctica and the deep sea.[8,9] The composition and size range of microplastics sampled in the environment and the underlying transport mechanisms are important to model the fate of microplastics in the future and propose solutions for this urgent environmental problem. However, our understanding of microplastics is strongly constrained by the analytical methods currently available.[10–12] For the transport of MPPs in the environment, their colloidal and interfacial properties at the solid/liquid interface are highly important.[3,7,13–19] To date, nearly all studies on the solid/liquid interface of MPPs have relied on model systems composed of small micrometer-sized particles that were obtained by suspension polymerization and

M. B. Engelhardt, N. Helfricht, G. Papastavrou
Department of Physical Chemistry II
University of Bayreuth
95447 Bayreuth, Germany
E-mail: georg.papastavrou@uni-bayreuth.de

D. Wagner, S. Agarwal
Department of Macromolecular Chemistry II
University of Bayreuth
95447 Bayreuth, Germany

M. Zarebanadkouki
Department of Soil Biophysics and Environmental Systems
Technical University of Munich
85354 Freising, Germany

N. Meides, P. Strohriegl
Department of Macromolecular Chemistry I
University of Bayreuth
95447 Bayreuth, Germany

C. Schulbert
Geozentrum Nordbayern
Section Palaeontology
Friedrich-Alexander-University Erlangen-Nürnberg (FAU)
Loewenichstraße 28, 91054 Erlangen, Germany

M. G. J. Löder, C. Laforsch
Department of Animal Ecology I
University of Bayreuth
95447 Bayreuth, Germany

A. Carminati
Institute of Terrestrial Ecosystems
ETH Zürich
8092 Zürich, Switzerland

J. Senker
Department of Inorganic Chemistry III
University of Bayreuth
95447 Bayreuth, Germany

Supporting information for this article is available on the WWW under https://doi.org/10.1002/cmtd.202500102

have diameters smaller than 5 μm.[11,14,17,20–24] By contrast, the best-studied size range of environmental microplastics is around 50 μm to 1 mm.[10–12,25,26] Larger particles are not only easier to sample in the environment,[27–29] but they are also a natural part of the weathering and degradation sequence of plastics in the environment, which starts with macroscopic plastic foils, tires, or bottles.[30,31] Moreover, there are strong indications that the weathering of small MPPs obtained by suspension polymerization differs significantly from the artificially fragmented particles.[32] This size mismatch between model systems and environmentally dominant MPPs limits the transferability of existing interfacial data to real-world scenarios. Hence, there is currently a great demand to study the solid/liquid interface of large MPPs. Here, we present, to the best of our knowledge, the first approach to studying the aging of MPPs by streaming potential measurements.

Practically all inorganic and organic surfaces immersed in aqueous electrolyte solution carry charges, either by ionization of functional groups or by ion adsorption.[33] In consequence, the ion distribution at the interface is very different from that of the bulk solution; an effect that is long known in colloid and interface science as the electrical double layer.[33,34] One distinguishes between the so-called Stern-layer of strongly adsorbed, thus practically immobile ions, which extends only 1–2 nm from the interface, and the diffuse layer where the counterion concentration is enhanced and decays exponentially from the interface.[33,34] The measurement of diffuse layer properties is often essential, as they play an important role in the stability of colloidal suspensions in the framework of the so-called DLVO theory.[33,34] For MPPs, their diffuse layer properties determine not only their aggregation and adsorption behavior[14,20,24,35] but also their interaction with natural organic matter.[36–38]

Due to the importance of the diffuse layer properties in colloid science, the development of suitable analytical techniques for their characterization has been pursued for over a century. For small colloidal particles, the diffuse layer is commonly studied by the measurement of the electrophoretic mobility in an external electric field.[10,16,17,39–43] During the resulting particle movement in the viscous electrolyte solution, a significant part of the diffuse layer is sheared off and one measures the particle's velocity, which is directly connected with the so-called zeta-potential ζ, which is directly related to the diffuse layer potential and thus the surface charges.[44] However, in order to utilize electrophoretic mobility, the particle diameters must be well below 30 μm,[40] and even 10 μm.[45] Electrophoretic mobility measurement is widely used in MPP research.[18,19,46–48] For flat substrates, the so-called streaming potential measurements provide access to the zeta-potential. In this case, the flat substrate remains fixed, and the electrolyte solution is streamed over the substrate while the resulting potential due to the displacement of the ions is measured. The measurement of the streaming potential can be considered as "inverse" technique to electrophoretic mobility.[40,44] The basic principle of streaming potential measurements dates back more than 150 years.[49] Commonly, the streaming potential technique today is used with a channel made up of two macroscopic parallel plates.[50–61]

Considering the available techniques, it is no surprise that the diffuse layer of large MPPs liquid/solid interface remains largely a "blind spot" for analytics. By contrast, numerous analytical techniques are available to study the surface chemistry on the molecular level, also for large MPPs, such as Fourier transform infrared (FTIR) spectroscopy,[10,11,62,63] Raman spectroscopy,[10,11,24,64] scanning electron microscopy with energy-dispersive X-ray spectroscopy (SEM-EDX),[10,11,65–67] and nuclear magnetic resonance (NMR) spectroscopy.[63,66,68,69]

However, how can one determine the diffuse layer properties of particles that are too large to migrate in an external electric field, since sedimentation dominates, or that deviate from an ideal spherical shape, for example, of fibers or due to fragmentation processes? The primary answer was given already more than 60 years ago by introducing the so-called plug cells filled with beads or fibers in a defined confinement.[70,71] The streaming potential measured over such a particle or fiber plug allows the determination of its zeta-potential[70,71] also for large particles with irregular shapes.[72] Unfortunately, this technique has largely fallen out of focus in interface and colloid sciences. Notably, the use of streaming potential for characterizing large immobile particles was somehow not generally followed up in colloid science after some initial studies in the 1990s,[73–76] with some exceptions in recent years.[77,78] By contrast, the streaming potential technique has been widely used in soil science.[79–81]

This study demonstrates that streaming potential measurements are well-suited for characterizing large colloidal particles that would otherwise sediment and are therefore not accessible by electrophoretic mobility measurements. The specific application studied here is MPPs that have been prepared by mechanical fragmentation. Their change of surface chemistry during artificial weathering has been monitored by streaming potential measurements.[68,82–86] The knowledge about the solid/liquid interface of such MPPs is crucial for understanding their environmental fate and aging processes. The surface chemistry during environmental weathering is particularly important, as MPPs often originate from the breakdown of millimeter-sized plastic items.[30,31] Here, we demonstrate how streaming potential measurements can be used to determine the surface charge properties of large MPPs, which is impossible with "standard" techniques used for small particles as synthesized by suspension polymerization. For this study, we directly connected to a previous study based primarily on NMR measurements to characterize the surface of artificially weathered, fragmented MPPs.[66] While NMR and SEM-EDX are sensitive to the molecular composition, the here-presented technique probes the Stern and diffuse layer at the solid/liquid interface and thus reveals information about the ionization behavior at the surface. In order to provide a quantitative evaluation, we demonstrated that the streaming potential protocol used here was largely independent of the size fraction by studying artificially fragmented poly(styrene) particles ranging from 200 to 20 μm. The limits in terms of identifying functional groups by their titration behavior were verified by comparing the streaming potentials for commercial spherical particles with different surface functional groups.

2. Results and Discussion

In this study, we concentrated primarily on artificially fragmented MPPs. These particles were artificially weathered through simulated solar exposure combined with simultaneous mechanical stress by stirring.[66] Our source polystyrene (PS) material, the fragmentation, and the weathering process are fully analogous to the study performed by Meides et al. (2021) with a complementary set of analytical techniques that concentrated primarily on the molecular composition at the MPP surface.[66] The weathering process did lead to a significant reduction in particle size for artificial weathering times of up to 3200 h. Hence, we verified how far the particle size distribution affected the streaming potential by comparing different size fractions before artificial weathering. Moreover, commercial spherical particles bearing various functional groups at the surface have been studied to corroborate the technique's sensitivity to different functional groups.

2.1. Particle Size and Morphology

The following size fractions of fragmented MPPs from PS were studied: 1) 20–75 µm, 2) 75–125 µm, and 3) 125–200 µm. Fractionation was carried out by sieving after fragmentation.[66] The particle size distributions for three different size fractions of the fragmented PS particles were determined by laser diffraction (**Figure 1**a). All fractions showed rather broad size distributions, which were partially overlapping. The evaluated mean diameters from the Gaussian fits are listed in Table S1, Supporting Information. The size fractionation was corroborated by imaging with SEM, as shown in Figure 1b. These exemplary SEM images were acquired at the same magnification, illustrating the difference between the different size fractions. The smallest size fraction appears to have more elongated fragments than the larger fractions. More SEM images of the fragmented particles are shown in Figure S1–S3, Supporting Information. As expected, fragmentation induced considerable roughness on the nanoscale (Figure 1c). Further atomic force microscopy (AFM) images in Figure S4–S6, Supporting Information, highlight the observed variability of the topography on the nm-level. As the fragmented particles did show generally pronounced nonspherical shapes (Figure 1b), we additionally analyzed spherical particles. These were commercially available PS particles synthesized by suspension polymerization. The first batch of bare, spherical PS particles had a nominal diameter of 29.32 µm. Moreover, we studied spherical PS particles with diameters of ≈15 µm carrying three different chemical surface terminations (bare, amino-, and carboxy-modified). The corresponding SEM data can be found in the SI (Figure S7–S10 and Table S2, Supporting Information).

2.2. Particle Beds for Streaming Potential Measurements

Electrophoretic mobility measurements are commonly used to determine the zeta-potential of colloidal particles, relying on their movement under an external electric field. However, this technique becomes impractical for larger particles, such as microplastics, due to gravitational sedimentation and insufficient Brownian motion.[13,17,21,51] Large particles cannot migrate in a controlled manner in an external electric field as they sediment. Moreover, the light scattering for such large particles is not suitable anymore for the standard dynamic light scattering setups with an autocorrelator as commonly used in commercial instruments. For microplastics, particles with diameters larger than 5 µm fall in these regimes. Hence, a different approach to determine the zeta-potential of such particles has to be followed: streaming potential measurements. During those measurements, the large particles rest immobile while the electrolyte is streamed around them. To immobilize the particles during measurement, they are encapsulated in a so-called particle plug that is schematically shown in **Figure 2**a. The two electrodes measure the streaming potential and current, respectively, when the liquid passes through the particle plug. For particle plugs, the works of Lyklema and coworkers[87–89] and of Jacobasch and coworkers on textile fibers have to be mentioned.[90,91] In the following, we refer to the slightly compressed particle ensemble as the "particle bed". Such particle beds remained here largely intact after removal and allowed for further studies, e.g., by X-ray microtomography (µCT). Figure 2b shows a photograph of a typical particle plug removed from the cell after the measurement.

The particles must be homogeneously distributed within the particle bed for accurate streaming potential measurements. Inhomogeneous distributions or the presence of channels without particles could lead to significant deviations in the zeta-potentials.

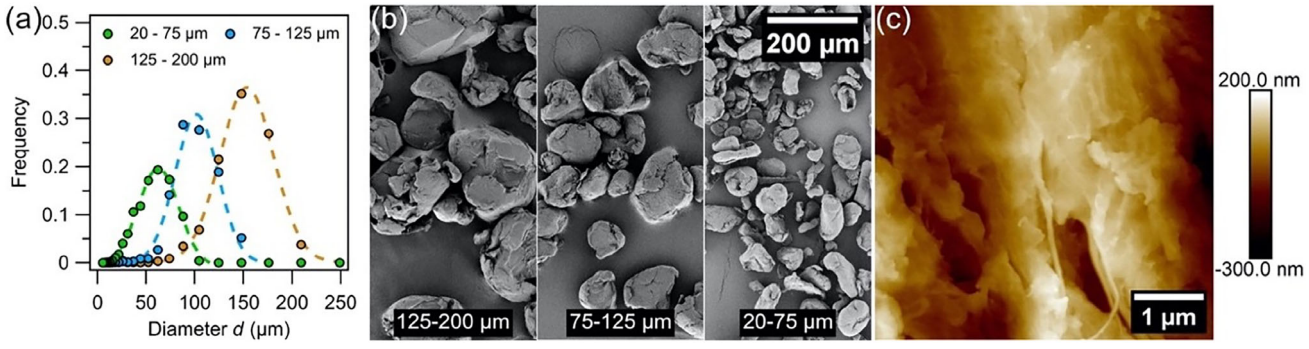

Figure 1. Size- and topography-related overview of fragmented polystyrene MPPs. a) Particle size distributions of different size fractions as determined by laser diffraction. b) Exemplary SEM micrographs of particles for the different size fractions. c) Exemplary (5 × 5) µm² AFM topography of a particle surface from the largest size fraction with 125–200 µm.

Research Article
doi.org/10.1002/cmtd.202500102
Chemistry Europe
European Chemical Societies Publishing

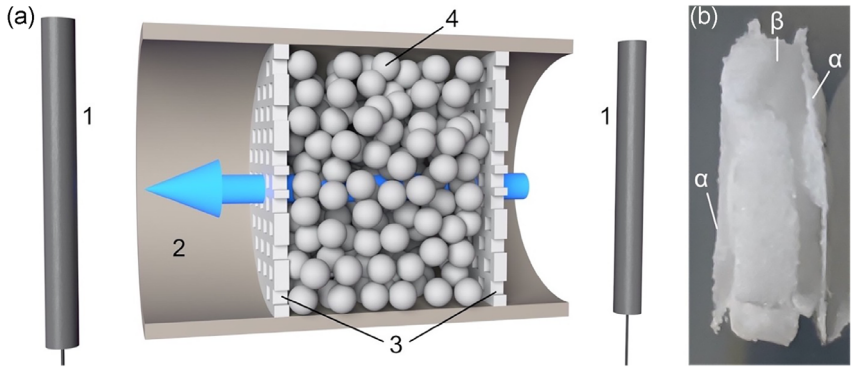

Figure 2. a) Schematic of a particle plug cell for the streaming potential measurements. The streaming potential was measured between the two Ag/AgCl electrodes (1). An outer cylindrical body machined from polyether ether ketone (PEEK) (2) and two PA-6,6 filter mats (3) encapsulate the particle bed (4), which is formed by randomly packed MPPs. The perforated bottom of the cylindrical body and the perforated stamp are not depicted for simplicity. The blue arrow indicates the liquid flow through the particle plug. b) Photograph of a particle plug after streaming potential measurements. (α) Represents the PA-6,6 filter mats around the plug and (β) shows the MPPs forming the particle bed. The particle plug had approximately a diameter of 10 mm and a thickness of 3 mm.

In particular, the formation of so-called seepage could lead to artifacts.[92] While Figure 2b demonstrates that the particle plugs had a dense appearance, their internal structure could not be resolved by optical methods. To evaluate the state of the particle beds after the measurements, we imaged some exemplary ones by μCT.[93,94] **Figure 3** shows the reconstructions of a particle bed from commercial spherical particles with a nominal approximate diameter of $d_{nom} = 30$ μm synthesized by suspension polymerization (Figure 3a) and an analogous reconstruction for fragmented PS particles originating from the 20–75 μm size fraction (Figure 3b). The 3D reconstructions were calculated from data acquired by a dedicated μCT scanner with a 180 kV nanotube without any filter applied. Scanning resolution was 1.5 μm at 50 kV and 200 μA current.

The μCT reconstruction of the particle bed with the spherical PS particles demonstrated not only their highly spherical shape and uniform size distributions but also corroborated that no deformations of MPPs due to compression in the particle plug (Figure S7, Supporting Information) took place. There were no indications for the formation of large seepages, and quantitative data evaluation yielded a solid volume fraction of 56.3% for the commercial spherical PS particles. This value was below the value for the densest possible hexagonal packing of equally sized spheres of 74% but indicated nevertheless dense particle packing. Further reconstructions for these particle beds by μCT are given in the SI (Figure S11, Supporting Information). By contrast, the reconstruction of the particle beds with fragmented MPPs of the size fraction 20–75 μm illustrated their irregular shape and the much broader size distribution (Figure 1b and S1, Supporting Infirmation). However, a dense packing was observed for these irregular particles. Moreover, additional μCT reconstructions are given in the SI (Figure S12, Supporting Information).

2.3. Electrokinetic Characterization of the Spherical Particles

The streaming potential originates from the dislocation of charges in the diffuse layer at the solid/electrolyte interfaces of the particles within the particle plug.[40,95] The extension of the diffuse layer is given by its exponential decay constant, the Debye length κ^{-1}.[33,44,95] The inverse Debye length κ is given by

$$\kappa = \sqrt{\frac{2e^2 N_A I}{\varepsilon_r \varepsilon_0 kT}} \tag{1}$$

where N_A is Avogadro's number, e the elementary charge, T the temperature, k the Boltzmann constant, I the ionic strength,

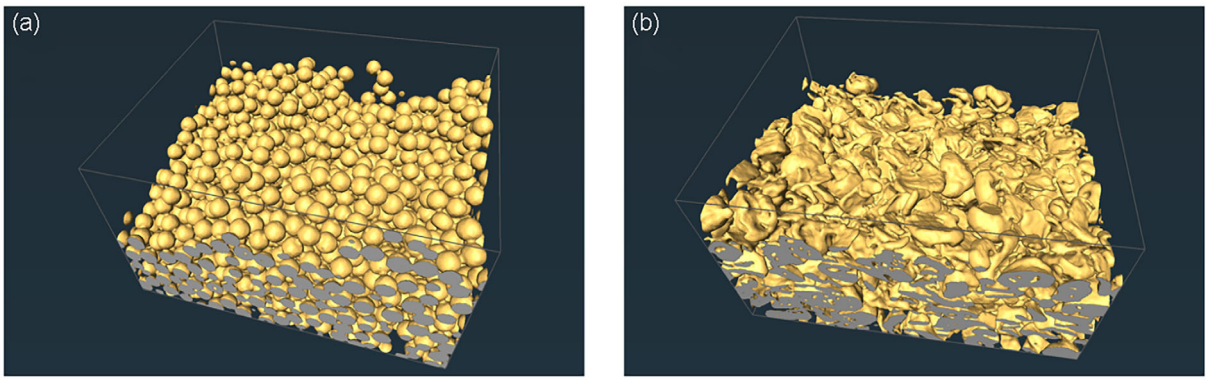

Figure 3. Reconstructed particle beds by X-ray μ-tomography. a) Reconstruction for commercial polystyrene particles with a nominal diameter of about 30 μm, which have been synthesized by suspension polymerization. b) Reconstruction for fragmented polystyrene particles with diameters in the range of 20–75 μm.

ε_r the permittivity of the electrolyte, and ε_0 is the permittivity of free space.[33,95]

The flow due to the externally applied hydrostatic pressure difference Δp displaces the counterions in the diffuse layer, which results in an electric current, the so-called streaming current I_{str}. Under open-circuit conditions, the resulting charge transport leads to an accumulation of opposite charges at the two ends of the capillary, which corresponds to a potential difference ΔU_{str}, the so-called streaming potential.[44] For sufficiently large capillary radii h and high ionic strengths I with $\kappa h >> 10$, the zeta-potential ζ is given by:[40,44,95]

$$\zeta = \frac{\eta K_L}{\varepsilon_r \varepsilon_0} \frac{\Delta U_{str}}{\Delta p} \tag{2}$$

where η is the dynamic viscosity of the electrolyte and K_L is its bulk conductivity. Equation (2) is also valid for porous plugs as long as the double layer relaxation effects and surface conduction can be neglected,[40] which is commonly the case for $\kappa r_{eff} >> 100$ with r_{eff} as the effective pore radius.[75] The effective pore radius r_{eff} can be calculated by[76]

$$r_{eff} = \left(\frac{\phi}{(1-\phi)}\right) \frac{d_{sv}}{4.5} \tag{3}$$

where ϕ is the porosity of the plug and d_{sv} is the surface volume mean diameter of the particles. ϕ can be determined from µCT evaluations. In the case of Figure 3a, one obtains for $I = 10$ mM and a particle diameter $d = 29.32$ µm for the spherical particles packed with $\phi = 1 - 0.563 = 0.437$ (evaluation of Fig. S11, Supporting Information) the estimation $\kappa r_{eff} \cong 1661$. Additionally, the zeta-potential ζ becomes independent from the details of the plug geometry and the particle shape for $\kappa r >> 100$.[75,96] We assume that this condition (i.e., $\kappa r >> 100$) has been fulfilled for all particle beds studied here by streaming potential measurements (Figure 3). It should be noticed that for hydrophobic particles an additional factor, the so-called hydrodynamic slip effect in pressure driven flows, can contribute.[97,98] However, this effect has not been considered here.

2.4. Influence of Functional Groups on Streaming Potential of Small Spherical Particles

In the following, we verified that streaming potential measurements with particle beds are indeed sensitive to the surface chemistry of the particles. This initial evaluation of the particle beds was based on spherical PS-particles of the same diameter, namely ≈15 µm, which have been synthesized by suspension polymerization. While the particles all have the same diameter, they carry different groups at their surface, namely bare PS and particles modified with carboxylic groups (PS-COOH), and amino groups (PS-NH_2), respectively. Thereby, the zeta-potentials ζ (Equation (2)) as a function of pH could be acquired for functional groups whose ionization behavior should differ. The particle diameters have been verified by SEM-imaging (Figure S7–S10 and Table S2, Supporting Information).

Figure 4 compares the zeta-potentials ζ as a function of pH for the small spherical PS-particles with different surface functional groups. In the acidic regime, the bare and COOH-modified PS particles started both at streaming potentials near 0 mV. This corresponds to very low surface charge densities and, thus, ζ according to the modified Grahame equation, where the charge density at the plane of shear σ_{ek} is set in relation to ζ for the planar limiting case.[99]

$$\sigma_{ek} = \frac{2\varepsilon_r \varepsilon_0 kT\kappa}{e} \sinh\left(\frac{e\zeta}{2kT}\right) \tag{4}$$

Upon increase of pH, the bare PS particles and the ones with COOH-groups develop more negative zeta-potentials in the basic regime. For the carboxylic groups at the particle surface, such a behavior was expected due to the deprotonation of the functional groups with $pK_a = 4.9$.[100] For the bare PS particles, which also develop an increasingly negative surface charge density, two other mechanisms were responsible: ion adsorption and

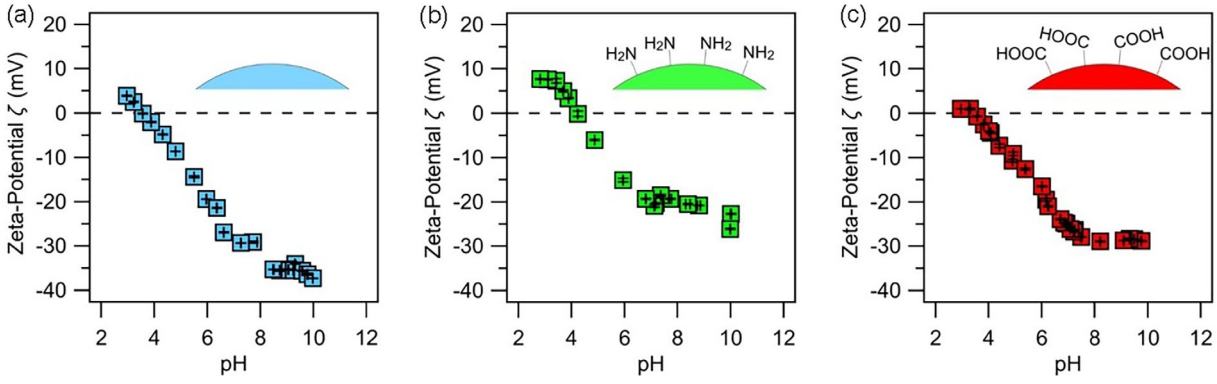

Figure 4. Zeta-potential ζ as a function of the pH for commercial a) PS, b) PS-NH_2, and c) PS-COOH particles synthesized by suspension polymerization as model systems for MPPs with different functional groups. The data were acquired by streaming potential measurements for particles with a diameter of ≈15 µm. The total ionic strength was 10 mM for all measurements.

ionization of the remaining initiator molecules. These mechanisms will be discussed in more detail below. By contrast, the amino-modified particles are positively charged under acidic conditions, as it would be expected from the protonation of the NH_2-groups, which are assumed to have a pK_a in the range of 8–11, depending on the electrical environment of the amino groups.[101,102] However, with increasing pH, negative surface charges also accumulate by the same mechanisms as for the bare PS particles. Thus, PS-NH_2 also showed negative zeta-potentials in the basic regime, but less than those for PS-COOH or bare PS.

It is important to highlight that negative charges accumulate on bare PS particles without any ionizable groups. The adsorption of hydroxyl-ions (OH^-) to hydrophobic surfaces is well known in the literature.[58,61,103,104] It has been observed for flat surfaces as well as for colloidal particles.[58,61,104] Furthermore, specific adsorption of predominantly anions to the apolar regions on PS particles is another factor leading to an overall more negative surface charge.[16,105] The presence of ionizable groups, here -COOH and -NH_2, reduces ion adsorption effects.[91,106] Additionally, the residues from the organo-sulfate initiators used in the polymerization can be often traced on the particles,[18,104,107–110] which are another source of negative charges and shift the isoelectric point (IEP) in the more acidic regime.[57,60,61,111,112]

PS-particles are often sterically stabilized by a layer of polyvinyl alcohol (PVA).[113] A soft polymeric layer shifts the shear plane further away from the interface, leading to zeta-potentials of smaller magnitude.[55,95,114,115] PVA around the particles also influences the specific ion adsorption of predominantly anions to the interface. PVA is more hydrophilic than PS, which leads to reduced specific anion adsorption in the basic regime.[91,106] AFM micrographs of the PVA-coated surface of nonmodified particles with diameters of 15 μm are shown in Figure S13, Supporting Information. The topographies reveal thick layers of PVA, creating a crater-like surface. In turn, a strong shift of the shear plane away from the interface must be assumed, leading to smaller zeta-potentials in magnitude. Another factor to consider is the PA-6,6 filter mats, which hold all the presented particle plugs in place. Hence, these filter mats (Figure S14b, Supporting Information), which were present in all measurements, have been characterized in a set of separate measurements. Figure S14a, Supporting Information shows the streaming potential measurements of a set of filter mats without particles. These measurements do not serve strictly as a baseline as a sufficient number of these mats had to be assembled. The streaming potential versus pH differs from those acquired for the PS particles and MPPs. Figure S14b, Supporting Information presents an exemplary SEM image of a cleaned filter mat.

2.5. Electrokinetic Characterization of Microplastics after Fragmentation

The fragmentation process produced MPPs with broad size distribution (Figure 1a) and irregular shapes (Figure 1b).[66,116] Due to their size, such particles cannot migrate in an electric field without sedimentation. Streaming potential measurements using packed particle plugs were the only feasible method to determine their diffuse layer properties, i.e., the zeta-potential ζ. As all size fractions studied here show lateral dimensions in all axes with $r > 7.5$ μm, hence, the condition $\kappa r >> 100$ is fulfilled at a total ionic strength $I = 10$ mM with $\kappa^{-1} \simeq 3$ nm, which was the ionic strength I at which the streaming potential measurements were carried out. To verify that the resulting streaming potential was independent of the particle size and geometry under these conditions, we studied the three different size fractions of the artificially fragmented PS. The particles were prepared from one fragmentation experiment and selected by size through sieving, so their surface chemistry was comparable. For further comparison, we also performed experiments with commercial spherical PS particles with diameters of ≈30 μm (Figure S7d–f, S10b, and Table S2, Supporting Information), which were produced by suspension polymerization. Their diameter falls nicely within the size range of the smallest fragment fraction, but the particles provided a highly defined, non-varying geometry, and a smoother surface. μCT images of the corresponding particle beds are shown for these particles in Figure 3a and for the fragmented particles in Figure 3b.

Figure 5a shows the zeta-potential as a function of pH for the spherical model PS particles (30 μm in diameter). For low pH, i.e., pH < 4, the zeta-potential was slightly positive with an IEP between pH 3 and 4. Upon increasing the pH, the zeta-potential becomes more negative without reaching a plateau value in the basic regime (pH ≲ 10) compared to the smaller particles (Figure 4a). The discrepancy in zeta-potentials between Figure 4a and 5a is likely attributed to the different amounts of PVA-coating of the particles. The particles with nominal diameters $d_{nom} = 15$ μm appear to be heavily coated with PVA, while the particles with $d_{nom} = 30$ μm are less coated (Fig. S15, Supporting Information). A thicker PVA coating shifts the shear plane further away from the PS interface compared to a thinner coating, thus leading to smaller zeta-potentials in comparison.

Figure 5b shows the zeta-potential as a function of the pH for the three size fractions of the fragmented MPPs. The overall shape of the curves was practically independent of the size fraction. This experimental finding also corroborates the theoretical postulate that for particle dimensions with $\kappa r >> 100$, the zeta-potential even becomes independent from the details of the plug geometry and the particle shape.[75,96] Moreover, we find a surprisingly good correspondence in the surface titration behavior between highly defined spherical bare PS particles with low amounts of PVA at the interface and the fragmented particles obtained from solid PS. The IEP was slightly more acidic, but the increase in the zeta-potential's magnitude with increasing pH followed the same trend observed for large colloidal particles. However, in the case of the fragmented particles, the zeta-potentials level off after pH 7–8 into a pronounced plateau.

2.6. Charging Mechanisms of the Polystyrene/Water Interface

The zeta-potential versus pH curves for spherical 30 μm sized PS particles and bare as well as aged MPP are surprising as polystyrene has in principle no ionizable groups. **Figure 6** illustrates schematically several different charging processes that can lead

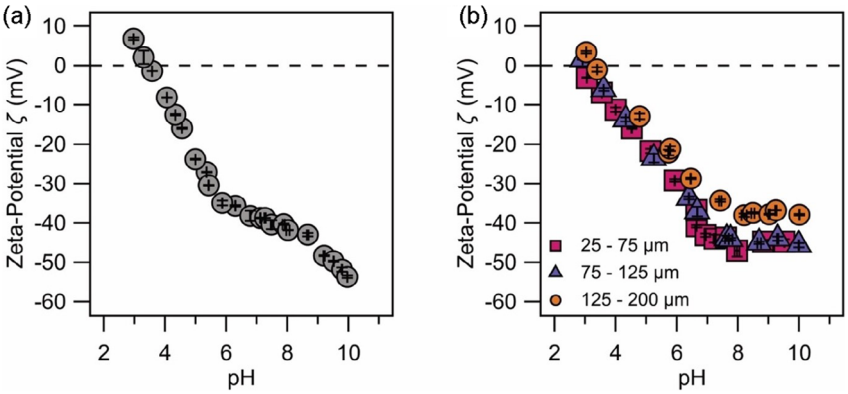

Figure 5. Zeta-potential as a function of the pH at a constant ionic strength of 10 mM in KCl for a) commercial polystyrene particles with $d \approx 30$ µm and b) fragmented microparticles of three different size fractions as determined by streaming potential measurements with a particle plug cell.

to the presence of charges at a PS-surface. The dominance of one mechanism or the presence of several mechanisms depends critically on several factors, particularly the origin of these PS particles. One process common to all types of PS solids is the presence of initiator molecules, which were necessary for polymerization and have not been fully consumed.[107] A schematic representation is shown in Figure 6a. For particles synthesized by emulsion polymerization, also surfactants, which were originally present in the solution to stabilize the emulsion droplets, can remain at the interface. Their hydrophilic groups are also charged and will accumulate at the particle's interface (schematic representation in Figure 6a). A different type of molecules are stabilizers, like polyvinyl alcohol, which were added to suspension polymerizations to increase the shelf life (Figure 6b). While the PVA-layer itself cannot directly accumulate charges, the shift of the shear plane and structural changes lead to the shift of the zeta-potential.[117] The stabilization of the suspension takes primarily place by steric interactions.[33] Nevertheless, negative charges can accumulate at PVA under alkaline conditions due to ion adsorption.

Surfaces from PS are generally hydrophobic.[118] For such surfaces, ion adsorption (Figure 6c) plays an important role, in particular by hydronium (H_3O^+) and hydroxyl ions (OH^-).[58,60,61,103,119] The corresponding charging processes on hydrophobic surfaces due to ion adsorption have been followed by streaming potential measurements as well as by direct force measurements by AFM in the past.[58,60,61,103,120] At low pH, i.e., under acidic conditions, the adsorption of hydronium ions is the dominating process.[52,60,61,103,119,120] However, the adsorption of hydroxyl ions is preferential at a hydrophobic surface already for pH > 4 to 7.[52,60,61,120] Hence, the IEP for nonmodified PS particles often lies around pH 4.[40] By contrast, the specific adsorption of hydrated ions, such as K^+ and Cl^-, does practically not contribute to hydrophobic polymer interfaces[60] or molecularly defined hydrophobic self-assembled monolayers (SAMs).[120]

Additionally, the presence of organosulfates due to the remaining traces of the polymerization initiator can have a significant contribution to an overall negative surface charge due to the deprotonation of sulfate groups.[104,108–110] The mechanism is indicated in Figure 6a. Such sulfate groups are more present on the spherical particles synthesized by suspension polymerization than on the fragmented pristine PS. The thinner PVA-coating of the 30 µm sized particles compared to 15 µm sized particles, as deducted from the AFM imaging (Figure S15 and S13, Supporting Information, respectively), would be compatible with the zeta-potentials resembling that of the fragmented PS rather than the one observed for bare 15 µm sized particles. The observed differences can be attributed to the remaining initiator molecules on the surfaces of the 30 µm sized PS particles. By contrast for the MPP obtained by fragmentation, the presence of peroxides from initiator leftovers[121] and due to photo-oxidation/reduction can attribute to the surface charge (Figure 6d).[122] However, the peroxides generally contribute at much higher pH than the processes illustrated in Figure 6a-c.

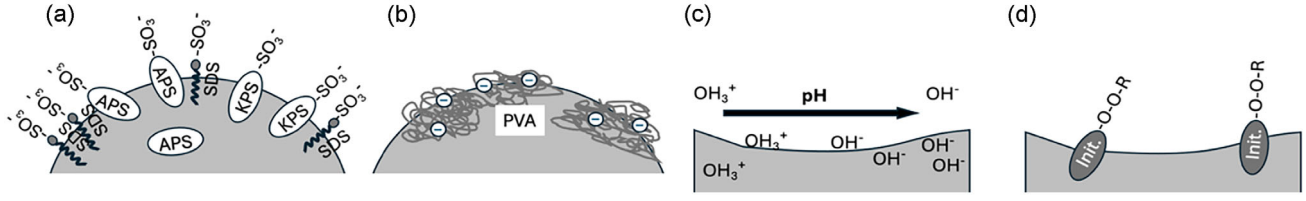

Figure 6. Schematic representation of the different charging processes for polystyrene surfaces. a) Charges due to the presence of remaining initiators such as (APS) and (KPS) as well as surfactants from emulsion polymerization. b) Polyvinyl alcohol as a steric stabilizer for particles synthesized by suspension polymerization. Under alkaline conditions, negative charges can be present on the PVA. c) Ion adsorption, especially of hydroxyl ions. This effect is more pronounced for a flat surface without any ionizable groups. d) For the bulk material PS, as used for the fragmentation procedure, some initiators bearing peroxides remain unreacted.

2.7. Artificial Weathering of the Microplastic Particles

Artificial weathering of fragmented PS (125–200 μm size fraction) was carried out by stirring and intense UV exposure of the aqueous suspension. Here, we used samples from the identical batches previously studied by Meides et al., which have been examined by SEM, laser scattering, and NMR spectroscopy.[66] We added streaming potential measurements to the original analytical selection to provide additional information on the level of the diffuse layer properties.

Figure 7a shows the size distribution of the fragmented PS for exposure times of 0, 600, 1200, and 3200 h to artificial weathering as reported previously.[66] Mean diameters after weathering exposure are shown in Table S3, Supporting Information. In this study, the identical batches studied by Meides et al. (open data points) have been used with the exception of the one for 0 h (closed data points). Nevertheless, the original size distribution for 0 h from Meides et al. has been added for comparison. The difference in the size distribution for these two batches at 0 h weathering time was found to be small. The artificial weathering process leads to a reduction in the particle size with time. For the longest exposure time, an average size reduction to 85% of the original was observed (Figure 7a). In consequence, the overall size distribution is comparable to the smallest size fraction of pristine, fragmented PS-particles of 20–75 μm (Figure 1a). This comparison will become important at a later point in order to exclude size effects on the here-determined streaming potential for weathered particles.

Figure 7b shows the zeta-potential ζ as a function of pH for the particle plugs prepared from the MPPs at different weathering times. For 0 h, the ζ versus pH data are identical to the ones shown in Figure 5b. For up to 1200 h of artificial weathering, ζ (pH) remained practically identical to the curve acquired for 0 h weathering, including the position of the IEP. However, for 3200 h of artificial weathering, a general shift to more negative zeta-potentials took place. The final size distribution of the MPPs at this weathering time was very similar to the size fraction 20–75 μm (Figure 1a), which did show no change of ζ (pH) in comparison to the larger size fractions (Figure 5b). Hence, we assume that the size of the MPPs after 3200 h had no or only a very minor effect on ζ (pH). However, with increasing weathering time, the surface of the MPPs became significantly rougher. The former process can be directly followed by microscopy, such as SEM and AFM. Some exemplary results for SEM are shown in **Figure 8** and in Figure S16–S19, Supporting Information.

On a more local scale, the effect of artificial weathering on the particle surfaces becomes even more evident. **Figure 9** shows the particle surface topographies for the same weathering times. However, this time the surface topography has been determined by TappingMode AFM in air. The images shown are based on the phase data, which have been acquired simultaneously with topographic data. The former provided a good image of the surface ultrastructure as its first derivative entered the phase image contrast and allowed access to the chemical homogeneity based on differences in adhesion or elasticity. The phase images show a chemically homogeneous surface but with an increasing roughness on the nm-level with weathering time. The corresponding topography images can be found in Figure S20, Supporting Information and roughness data in Table S4, Supporting Information.

Hence, we attributed the observed shift primarily to changes in the surface chemistry of the MPPs during weathering. Which new groups at the surface of the MPPs can be responsible for the increasingly negative charge on the MPPs as the weathering progressed? Meides and coworkers investigated the same batches of weathered particles via SEM-EDX and NMR spectroscopy.[66] Their experiments show increased oxygen species, especially peroxides, carboxylic groups, and ketones with artificial weathering time. For interfacial carboxylic groups, one commonly assumes $pK_a = 4.9$,[100] while peroxides and ketones typically have a pK_a of > 7 and $\simeq 19$, respectively.[123,124] Due to their much higher pK_a-values, these groups should contribute significantly less to the overall negative charge. However, the carboxylic groups have a pK that would be compatible with the observed pH behavior and explain the increasing negatively charged surfaces in the neutral and basic pH-regime with aging time. An increase of carboxylic groups with weathering times was also observed by NMR spectroscopy. Hence, a technique that is sensitive to the

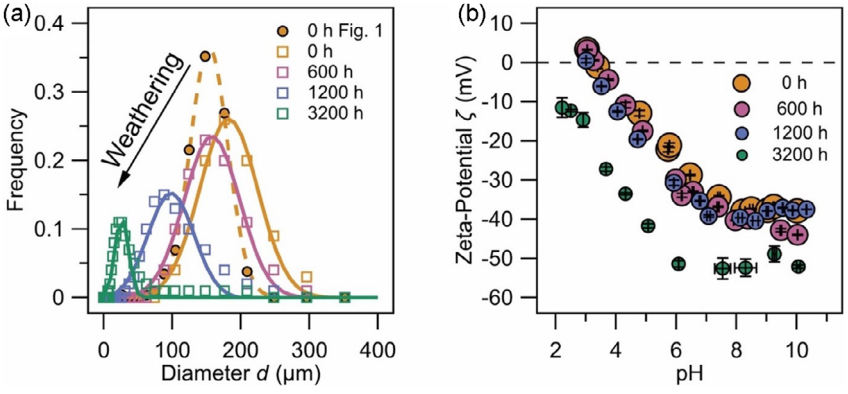

Figure 7. a) Size distribution of weathered microparticles (i.e., solid lines and open data points) as determined by laser diffraction from Meides et al.[66] and the non-weathered (i.e., 0 h) particles as shown in Figure 1 (dashed line, filled data points). b) Zeta-potential as a function of the pH at a constant ionic strength of 10 mM in KCl for weathered fragmented MPPs.

Research Article
doi.org/10.1002/cmtd.202500102
Chemistry Europe
European Chemical Societies Publishing

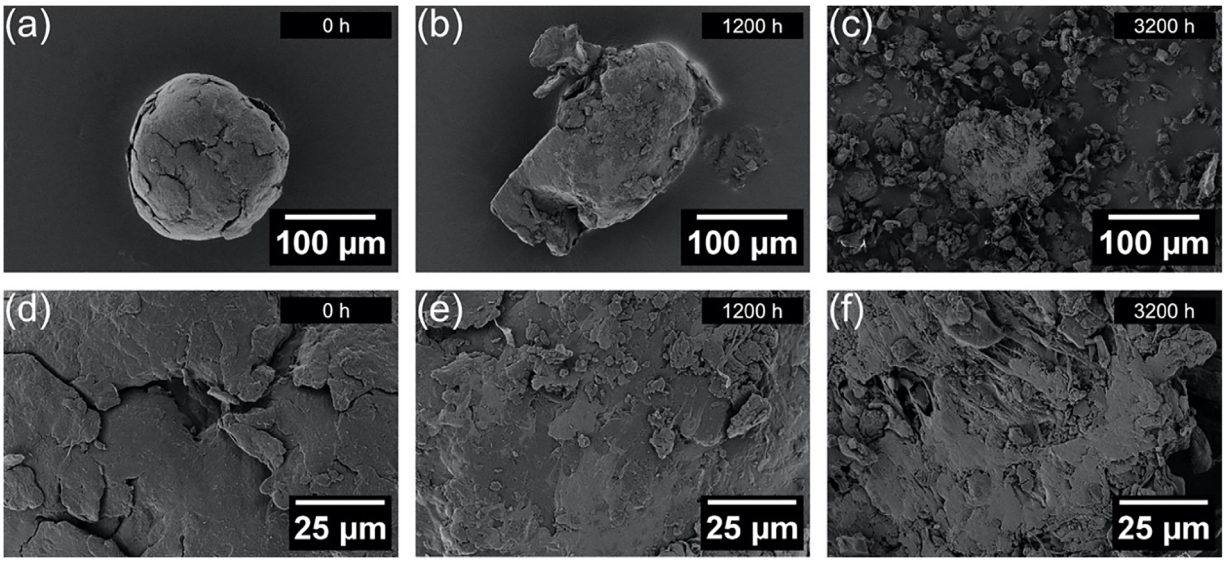

Figure 8. a,d) SEM images of fragmented, i.e., 0 h weathering and b,c,e,f) subsequently artificially weathered MPPs. The top row shows some exemplary particles for the different weathering times. The bottom row shows some ultrastructure on the particles shown in the top row.

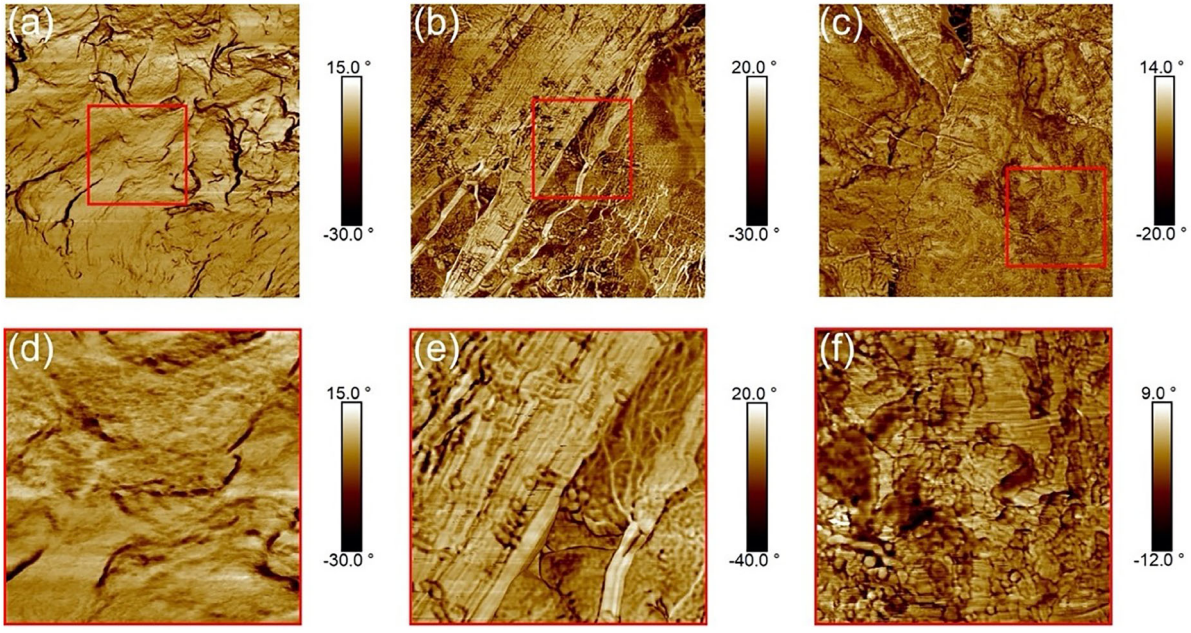

Figure 9. a,d) AFM images of fragmented, i.e., 0 h weathering and b,c,e,f) subsequently artificially weathered MPPs. The top row shows images with a scan area of $(3 \times 3)\ \mu m^2$. The bottom row shows some ultrastructure on the particles as indicated by the red squares with scan areas of $(1 \times 1)\ \mu m^2$. The AFM images have been acquired in TappingMode in air and only the phase image data are shown.

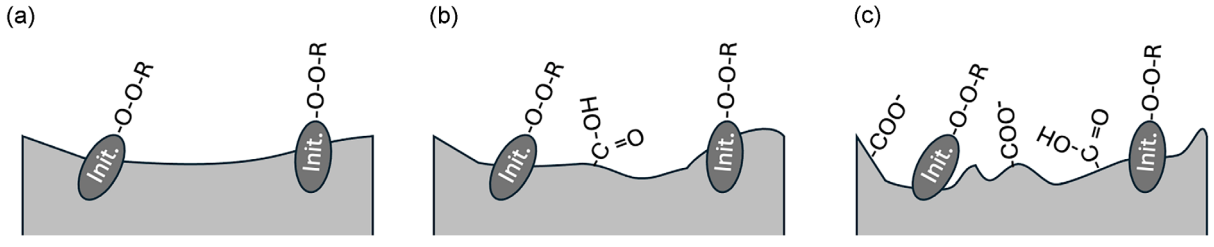

Figure 10. Schematic representation of the changes in the surface chemistry during the weathering of the polystyrene surfaces. a) Initial state of the surface. b) The artificial weathering did lead with increasing time to more charged groups, especially due to the formation of carboxyl groups. Moreover, not only was the size of the particles reduced, but their roughness was also increased. c) With increasing weathering, the number of carboxylic groups and the roughness increased.

molecular composition of the MPP's surface chemistry and a technique that probes the diffuse layer resulting from charges at the MPPs provide matching results.

Figure 10 summarizes the proposed changes at the MPP surface with aging. The density of the leftover initiator groups most likely did not change significantly, as these are present in the bulk for solid PS. Thus, degradation of the particles should lead to a more or less constant background of negative charges from the peroxides from the initiator groups. With increasing weathering time, the surface of the MPPs not only became rougher, but also the number of carboxylic groups increased, which is perfectly in line with the results previously reported by different techniques.[66]

3. Conclusions

Streaming potential measurements with particle plugs provide an analytical approach to determine the diffuse layer properties of large particles with irregular shapes. Such particles are not accessible by electrophoretic mobility measurements, which represent the standard technique to characterize colloidal particles with a diameter of less than 5 μm, since such particles rapidly sediment or float, making electrophoretic methods ineffective. Moreover, dynamic light scattering, which is often used for determining the electrophoretic mobility, would not provide reasonable results for large particle diameters. Streaming potential measurements are most often carried out for flat, cm-sized samples but can also be used for large particles or fibers. However, this analytical possibility has been largely ignored in the past decade in colloid and interface science. As we demonstrated here, particle plugs provide an important analytical method for a critical size regime in microplastic research. While many initial studies in this field have used small particles (<5 μm) synthesized by emulsion polymerization, these particles are not the dominant component of microplastics in the environment.[125] The here-studied weathering of larger plastic segments represents a much more relevant insight into the processes that determine the fate of microplastics in the natural environment and provides complementary information to techniques such as NMR spectroscopy for the molecular composition or microscopy for the particle dimensions and morphology.

Here, we demonstrated that the size of the MPPs does not play a role for the size range of 20–200 μm, which is in line with studies on smaller particles in particle plugs[73–76] and theoretical predictions.[75,96] Moreover, we showed that PS particles with defined functional groups (carboxylic, amino, and bare) but the same size do indeed lead to different zeta-potential versus pH curves as expected for these groups. However, for plastics, the presence of ion adsorption and the rest of the initiator and surfactant molecules lead to very similar charging curves in the neutral and acidic regimes. Due to the presence of steric stabilizers and more pronounced ion adsorption to bare PS particles obtained by suspension polymerization, these can accumulate more negative charges than those bearing carboxylic groups. This counterintuitive finding is also in line with studies on small colloidal particles by electrophoretic mobility measurements. It should be kept in mind that ion adsorption, especially of hydroxyl-ions, and remnants of initiators are omnipresent for plastic surfaces. Hence, the filter membranes that are used to constrain the particles in the filter plug also show a similar pH dependence as the plastic material under examination. Presently, we have no indication that the sensitivity of the streaming potential measurements would be affected thereby. Future studies should also address how far the reduction of hydrophobic slip might influence the streaming potentials of MPPs during aging.

Our findings for the aging of microplastics due to artificial weathering match the results from complementary techniques, such as NMR spectroscopy and SEM, for the same batches.[66] Streaming potential measurements allow direct determination of the zeta-potential, i.e., the most relevant property of the solid/liquid interface, of environmentally relevant microplastic surfaces. The zeta-potential has a large influence on the adsorption of natural organic matter as well as the adhesion of MPPs to sediments. Hence, we believe that this technique has a large application field in environmentally oriented research with artificial contaminants. Large MPPs are sampled routinely in environmental studies. Hence, it would be important to have analytical techniques that allow for the determination of their surface properties. In principle, the here-presented approach would also be suitable to study MPP samples from the environment. However, the presence of an ecocorona made up from natural organic matter and the requirement of having several mg of sample at disposition will severely restrict the application.

4. Experimental Section

Materials

Millipore-grade quality water (MilliQ IQ 7000, Merck KGaA, Darmstadt, Germany) was used for all cleaning processes and solution preparations. The total organic content of the water was always below 5 ppb with a specific resistivity of 18.2 MΩ cm. 1 M analytic grade hydrochloric acid and potassium hydroxide Titrisol ampoules (Merck KGaA, Darmstadt, Germany) and potassium chloride (BioUltra, Merck KGaA, Darmstadt, Germany) were used to prepare all aqueous electrolyte solutions. The pH value of these solutions ranged between pH 2 and pH 12 and was adjusted with KCl to an overall solution ionic strength of 10 mM.

Samples and Sample Preparation: Particles

Commercial spherical polystyrene particles with different surface modifications were obtained from microParticles GmbH (Berlin, Germany). These particles had either no surface functionalization (bare PS), amino groups (PS-NH_2), or carboxy groups (PS-COOH). The bare PS particles had nominal diameters of 15.10 μm, and 29.32 μm (Figure S7, Supporting Information). The modified polystyrene beads had nominal diameters of 15.47 μm (Figure S8 and S9, Supporting Information, respectively). The diameters were corroborated from the SEM images, and the results are summarized in Figure S10 and Table S2, Supporting Information. All commercial particles were received as aqueous suspensions.

Fragmented polystyrene particles were produced from commercially available Styrolution PS 158 N polystyrene pellets (INEOS Styrolution

Group, Frankfurt am Main, Germany) by a milling process. The pellets were precooled with liquid nitrogen, milled using an Ultra Centrifugal Mill ZM 200 (Retsch GmbH, Haan, Germany) with a 12-teeth rotor at 18,000 RPM, and subsequently sieved with an Alpine Air Jet Sieve E200 LS (Hosokawa Alpine AG, Augsburg, Germany).[66] The process was conducted in air and yielded particles with size ranges of 20–75, 75–125, and 125–200 μm, respectively. SEM images of these fractions are shown in Figure S1–S3, Supporting Information.

Samples and Sample Preparation: Artificial Particle Weathering

The 125–200 μm size fraction of the fragmented polystyrene particles was artificially weathered in water. Environmental weathering was simulated via sunlight irradiation and mechanical stress by stirring under ambient conditions for various exposure times. A detailed description of the preparation process of the fractionation as well as the weathering has been described previously.[66] Briefly, the weathering experiments were conducted in a Q-SUN XE-3 industrial test chamber (Q-LAB Corporation, Westlake, OH, USA). The irradiation source consisted of three xenon arc lamps, emitting radiation similar to natural sunlight, which was achieved using a Daylight-Q filter system (Q-LAB Corporation, Westlake, OH, USA), filtering out radiation with wavelengths below 295 nm. The irradiance was set to 60 W m^{-2} at wavelengths between 300 and 400 nm, corresponding to a total irradiance of 594 W m^{-2}.[66] The relative humidity was maintained at 50% and the chamber temperature was held at 38 °C. During irradiation, 20 g of the PS particle powder was constantly stirred in a quartz glass beaker containing 600 mL of deionized water. The water temperature was 55 °C, and the stirring was performed using a poly(tetrafluoroethylene) (PTFE)-coated magnetic stirrer at 150 rpm.[66] Particle samples were analyzed after 600, 1200, and 3200 h without further purification.

Methods: Scanning Electron Microscopy

In order to image the used PS MPP particles by SEM, commercial particle suspensions were spin-coated onto a clean silicon wafer piece at 2000 rpm for 60 s. The wafer piece was oxidatively cleaned as shown previously.[126] Afterward, the substrate was dried at 40 °C for 2 h in an oven. Fragmented particles were immobilized on conductive carbon adhesive pads (Plano GmbH, Wetzlar, Germany) and the pad was hardened for at least 12 h at ambient conditions. Before SEM imaging, a 1 to 2 nm thin layer of platinum was sputtered onto the sample using a sputter coater (Cressington 208HR, Cressington Scientific Instruments Ltd., Watford, UK). Imaging of the particles was performed using the secondary electron detector of a Zeiss LEO 1530 (Carl Zeiss Microscopy GmbH, Jena, Germany). The particle diameters of the spherical PS particles were quantitatively evaluated with the ImageJ software (Version 1.54f) and the built-in line tool.[127]

Methods: Laser Diffraction

In contrast, the particle diameters and size distributions of the fragmented and weathered PS particles were determined via laser diffraction with a Microtrac FlowSync particle size analyzer (Microtrac Retsch GmbH, Haan, Germany). This instrument uses laser diffraction (three lasers and two detectors) coupled with dynamic image analysis. Measurements were run as wet analysis using deionized water as the mobile phase. 2 to 5 mg of particles were added to 2 mL of 5 wt% $Na_4P_2O_7$ (Sigma Aldrich, St. Louis, USA) and a few droplets of Tween 20 detergent (Sigma Aldrich, St. Louis, USA) to avoid aggregation. This mixture was poured into the water-filled measuring cell and diluted with 200 mL of water. A 180 s ultrasound treatment (40 kHz) was further performed to ensure complete suspension of the particles. Mean values are generated from three measurements.

Methods: Atomic Force Microscopy

Samples for AFM measurements were prepared analog to SEM samples, except that no sputtering was performed. The topography of the fragmented PS particles was imaged by AFM using a Dimension Icon (Bruker Corp., Billerica, MA, USA) with a Nanoscope V controller in TappingMode under ambient conditions. OMCL AC160TS cantilevers (Olympus Corp., Tokyo, Japan) with a nominal resonance frequency of 300 kHz, a nominal tip radius of <10 nm, and a nominal spring constant of 26 N m^{-1} were used. AFM images were analyzed using the NanoScope Analysis software (Version 1.8, Bruker Corp., Billerica, MA, USA) with first-order plane fits applied.

Methods: Streaming Potential Measurements

Streaming potential experiments of the PS particles were conducted with a SurPASS 3 streaming potential analyzer and a cylindrical cell (Anton Paar GmbH, Graz, Austria). Streaming potential measurements involved the preparation of well-defined particle plugs of the polystyrene particles. Plugs were prepared with either spherical commercial, fragmented, or weathered particles. To immobilize the particle beds for streaming potential measurements, polyamide-6,6 (PA-6,6) filter mats with nominal pore diameters of 10 μm and an open surface area of 2% (Pieper Filter GmbH, Bad Zwischenahn, Germany) were used. Before usage, the filters were sonicated with a volumetric 3:1 solution of analysis grade isopropyl alcohol (VWR Chemical, Darmstadt, Germany) and water for 20 min at 40 °C. Afterward, the filters were sonicated in water for 20 min at 40 °C and dried under a nitrogen gas stream. An SEM image of the used PA-6,6 filter mats and a streaming potential reference experiment of a stack of six filters are given in the Supporting Information (Figure S14, Supporting Information).

Before the streaming potential measurements, the particle powder or suspension was filled in the cylindrical cell on top of a filter. The used particle mass was adjusted to a normalized surface area of ≈43 cm^2, given the assumption of spherical particles. Thus, the surface area of the particles was always comparable and it was ensured that the area was larger than the surface area of the PA-6,6 filters. The particle bed was first covered with a second filter mat, and the cell was sealed in the second step. The particle plugs were rinsed four times with 100 mL of the corresponding pH-adjusted solution before each measurement set. The electric conductivity of the solution and the temperature were recorded before each streaming potential experiment. The streaming potential measurements followed a pH titration protocol progressing from neutral to alkaline conditions and subsequently from neutral to acidic conditions. All streaming potential experiments were conducted at a constant total ionic strength of 10 mM in KCl across a pH range from 2 to 12. The experiments measured the streaming potential as a function of pressure, with the zeta-potential values calculated using the Helmholtz–Smoluchowski equation. The pressure range for the rinsing and streaming potential measurements was 600 to 400 mbar via a nitrogen gas stream. Four measurements were averaged per experiment after a stable zeta-potential was achieved. All streaming potential measurements were performed at a temperature of (295 ± 2) K.

Methods: X-Ray Microtomography

Samples were fixated on the top of a 2 mm thin glass rod and were immobilized using dental wax in order to be mounted in the beam

path of the μCT scanner at a distance of 6.3 mm to the focal point of the X-ray tube (FOD). The distance from the focal point to the detector (FDD) was 808 mm. For the scanning with the 180NF nanotube and a high-energy tungsten target at 50 kV/200 μA, we did not use any filters applied in the beam path. During a full revolution of the sample, we took 1500 2D projection images (acquired with a Phoenix DXR 250RT detector at 200 μm pixel size and 1.000 × 1.000 pixels). The reconstruction of the μCT images was performed with the Avizo software (Thermo Fisher Scientific GmbH, Schwerte, Germany). To distinguish the plastic particles from background and voids in the reconstructed volumes, image segmentation was performed using gray-scale thresholding in Avizo. The threshold values were determined empirically based on histogram analysis and visual inspection of representative slices. Due to the low X-ray attenuation contrast between the plastic particles and surrounding air, particular attention was paid to minimizing partial volume effects at the particle edges. A combination of non-local means filtering and contrast enhancement was applied prior to segmentation to reduce noise and enhance edge definition. The resulting binary masks were then validated against orthogonal slice views to ensure that particle geometry and pore structure were faithfully preserved, enabling reliable assessment of packing homogeneity and porosity relevant for interpreting streaming potential measurements.

Acknowledgments

The authors acknowledge the Keylab for Optical and Electron Microscopy at the Bavarian Polymer Institute (BPI). The authors are grateful to Nina Volk, Carmen Kunert, and Tamino Rößler for their help with the SEM measurements and to Markus Hund for his help with the AFM measurements. The authors also thank the GeoZentrum Nordbayern for providing μCT measurement facilities and Hao Liu from the University of Bayreuth for rating the quality of the μCT measurements. M.B.E. appreciates the support from the Elite Network of Bavaria (ENB) via the "Macromolecular Science" study program and the University of Bayreuth Graduate School. The authors thank Anika Mauel and the C01 project of the CRC 1357 Microplastics for providing the weathered MPPs. Open Access funding enabled and organized by Projekt DEAL. This work was funded by the Deutsche Forschungsgemeinschaft (DFG, German Research Foundation)—project no. 391977956—SFB 1357 (projects B01, B06, Z01, C01, and A04).

Open Access funding enabled and organized by Projekt DEAL.

Conflict of Interest

The authors declare no conflict of interest.

Author Contributions

Matthias B. Engelhardt: formal analysis (equal); investigation (lead); methodology (supporting); visualization (equal); writing—original draft (equal); writing—review & editing (equal). **Daniel Wagner**: formal analysis (supporting); investigation (supporting); methodology (supporting); writing—review & editing (supporting). **Mohsen Zarebanadkouki**: formal analysis (supporting); investigation (supporting); writing—review & editing (supporting). **Nora Meides**: investigation (supporting); resources (supporting). **Christian Schulbert**: investigation (supporting); methodology (supporting); writing—review & editing (supporting). **Martin G. J. Löder**: conceptualization (supporting); data curation (supporting); investigation (supporting); writing—original draft (supporting); writing—review & editing (supporting). **Nicolas Helfricht**: conceptualization (supporting); data curation (supporting); investigation (supporting); writing—original draft (supporting); writing—review & editing (supporting). **Seema Agarwal**: funding acquisition (supporting); methodology (supporting); resources (supporting); supervision (supporting). **Andrea Carminati**: funding acquisition (supporting); methodology (supporting); supervision (supporting). **Peter Strohriegl**: methodology (supporting); resources (supporting). **Jürgen Senker**: conceptualization (supporting); resources (supporting); supervision (supporting); writing—review & editing (supporting). **Christian Laforsch**: funding acquisition (equal); methodology (supporting); resources (supporting); supervision (supporting); writing—review & editing (supporting). **Georg Papastavrou**: conceptualization (lead); formal analysis (equal); funding acquisition (lead); methodology (lead); resources (lead); visualization (equal); writing—original draft (equal); writing—review & editing (lead).

Data Availability Statement

The data that support the findings of this study are available in the supplementary material of this article.

[1] Y. Chae, Y. J. An, *Environ. Pollut.* **2018**, *240*, 387.
[2] A. A. de Souza Machado, W. Kloas, C. Zarfl, S. Hempel, M. C. Rillig, *Glob. Change Biol.* **2018**, *24*, 1405.
[3] T. S. Galloway, M. Cole, C. Lewis, *Nat. Ecol. Evol.* **2017**, *1*, 116.
[4] R. Geyer, J. R. Jambeck, K. L. Law, *Sci. Adv.* **2017**, *3*, e1700782.
[5] S. Lambert, M. Wagner, *Microplastics Are Contaminants of Emerging Concern in Freshwater Environments: An Overview*, Springer International Publishing, Cham **2018**, 25.
[6] A. F. R. M. Ramsperger, E. Bergamaschi, M. Panizzolo, I. Fenoglio, F. Barbero, R. Peters, A. Undas, S. Purker, B. Giese, C. R. Lalyer, A. Tamargo, M. V. Moreno-Arribas, H. P. Grossart, D. Kühnel, J. Dietrich, F. Paulsen, A. K. Afanou, S. Zienolddiny-Narui, S. E. Hammer, T. K. Ervik, P. Graff, B. C. Brinchmann, K. C. Nordby, H. Wallin, M. Nassi, F. Benetti, M. Zanella, J. Brehm, H. Kress, M. G. J. Löder, C. Laforsch, *NanoImpact* **2023**, *29*, 100441.
[7] Y. Wang, L. Xiang, W. Amelung, M. Elsner, J. Gan, S. Kueppers, L. Christian, X. Jiang, J. Adu-Gyamfi, L. Heng, Y. S. Ok, N. P. Ivleva, Y. Luo, D. Barceló, A. Schäffer, F. Wang, *Trends Anal. Chem.* **2023**, *169*, 117309.
[8] A. R. Aves, L. E. Revell, S. Gaw, H. Ruffell, A. Schuddeboom, N. E. Wotherspoon, M. LaRue, A. J. McDonald, *Cryosphere* **2022**, *16*, 2127.
[9] M. Bergmann, V. Wirzberger, T. Krumpen, C. Lorenz, S. Primpke, M. B. Tekman, G. Gerdts, *Environ. Sci. Technol.* **2017**, *51*, 11000.
[10] Z. Huang, B. Hu, H. Wang, *Environ. Chem. Lett.* **2023**, *21*, 383.
[11] M. G. J. Löder, G. Gerdts, *Methodology Used for the Detection and Identification of Microplastics—A Critical Appraisal*, Springer International Publishing, Cham **2015**, 201.
[12] J. N. Möller, M. G. J. Löder, C. Laforsch, *Environ. Sci. Technol.* **2020**, *54*, 2078.
[13] Y. Adachi, L. Feng, M. Kobayashi, *Colloids Surf. A.* **2015**, *471*, 38.
[14] A. A. Harraq, B. Bharti, *ACS Environ. Au* **2022**, *2*, 3.
[15] A. Cramer, J. Schmidtmann, P. Benard, A. Kaestner, M. Engelhardt, S. Peiffer, A. Carminati, *Environ. Sci.: Process. Impacts.* **2023**, *25*, 1094.
[16] M. Elimelech, C. R. O'Melia, *Colloids Surf.* **1990**, *44*, 165.
[17] M. Kobayashi, M. Ookawa, S. Yamada, *J. Jpn. Soc. Civ. Eng., Ser. A2* **2014**, *70*, 743.
[18] A. F. R. M. Ramsperger, J. Jasinski, M. Völkl, T. Witzmann, M. Meinhart, V. Jérôme, W. P. Kretschmer, R. Freitag, J. Senker, A. Fery, H. Kress, T. Scheibel, C. Laforsch, *J. Hazard. Mater.* **2022**, *425*, 127961.

[19] S. Wieland, A. F. R. M. Ramsperger, W. Gross, M. Lehmann, T. Witzmann, A. Caspari, M. Obst, S. Gekle, G. K. Auernhammer, A. Fery, C. Laforsch, H. Kress, *Nat. Commun.* **2024**, *15*, 922.
[20] A. Amobonye, P. Bhagwat, S. Raveendran, S. Singh, S. Pillai, *Front. Microbiol.* **2021**, *12*, 768297.
[21] M. Kobayashi, *Colloid Polym. Sci.* **2008**, *286*, 935.
[22] B. Nguyen, D. Claveau-Mallet, L. M. Hernandez, E. G. Xu, J. M. Farner, N. Tufenkji, *Acc. Chem. Res.* **2019**, *52*, 858.
[23] W. J. Shim, S. H. Hong, S. E. Eo, *Anal. Methods* **2017**, *9*, 1384.
[24] Z. Sobhani, X. Zhang, C. Gibson, R. Naidu, M. Megharaj, C. Fang, *Water Res.* **2020**, *174*, 115658.
[25] J. L. Conkle, C. D. Báez D. Valle, J. W. Turner, *Environ. Manag.* **2018**, *61*, 1.
[26] A. Shamskhany, Z. Li, P. Patel, S. Karimpour, *Front. Mar. Sci.* **2021**, *8*, 760649.
[27] G. A. Covernton, C. M. Pearce, H. J. Gurney-Smith, S. G. Chastain, P. S. Ross, J. F. Dower, S. E. Dudas, *Sci. Total Environ.* **2019**, *667*, 124.
[28] C. Hung, N. Klasios, X. Zhu, M. Sedlak, R. Sutton, C. M. Rochman, *Integr. Environ. Assess. Manag.* **2021**, *17*, 282.
[29] F. Stock, C. Kochleus, B. Bänsch-Baltruschat, N. Brennholt, G. Reifferscheid, *Trends Anal. Chem.* **2019**, *113*, 84.
[30] D. K. A. Barnes, F. Galgani, R. C. Thompson, M. Barlaz, *Trans. R. Soc. B.* **2009**, *364*, 1985.
[31] P. Sethia, D. Nandhini, S. Amutha, *Mar. Ecol.* **2024**, *45*, 1.
[32] J. Schmidtmann, H.-K. Weishäupl, L. Hopp, N. Meides, S. Peiffer, *Environ. Sci.: Process. Impacts.* **2025**, *27*, 992.
[33] H. Butt, K. Graf, M. Kappl, *Physics and Chemistry of Interfaces*, Wiley-VCH, Weinheim **2003**.
[34] J. N. Israelachvili, *Intermolecular and Surface Forces*, Academic Press, Boston **1992**.
[35] A. Abdurahman, K. Cui, J. Wu, S. Li, R. Gao, J. Dai, W. Liang, F. Zeng, *Ecotoxicol. Environ. Saf.* **2020**, *198*, 110658.
[36] X. Wu, P. Liu, Z. Gong, H. Wang, H. Huang, Y. Shi, X. Zhao, S. Gao, *Environ. Sci. Technol.* **2021**, *55*, 15810.
[37] Y. Wang, P. Zhao, H. Yi, X. Tang, *Environ. Sci.: Process. Impacts.* **2025**, *27*, 849.
[38] Y. Chen, H. Tang, Y. Cheng, T. Huang, B. Xing, *J. Hazard. Mater.* **2023**, *455*, 131636.
[39] K. L. Chen, M. Elimelech, *Environ. Sci. Technol.* **2009**, *43*, 7270.
[40] A. V. Delgado, F. González-Caballero, R. J. Hunter, L. K. Koopal, J. Lyklema, *J. Colloid Interface Sci.* **2007**, *309*, 194.
[41] J. F. Duval, H. Ohshima, *Langmuir* **2006**, *22*, 3533.
[42] J. R. Martin, I. Bihannic, C. Santos, J. P. Farinha, B. Demé, F. A. Leermakers, J. P. Pinheiro, E. Rotureau, J. F. Duval, *Langmuir* **2015**, *31*, 4779.
[43] J. Stone-Masui, A. Watillon, *J. Colloid Interface Sci.* **1975**, *52*, 479.
[44] R. J. Hunter, *Zeta Potential in Colloid Science: Principles and Applications*, Academic Press, London **1981**.
[45] S. Antunez-Vela, V. H. Perez-Gonzalez, A. C. De Peña, C. J. Lentz, B. H. Lapizco-Encinas, *Anal. Chem.* **2020**, *92*, 14885.
[46] A. A. Harraq, P. J. Brahana, O. Arcemont, D. Zhang, K. T. Valsaraj, B. Bharti, *ACS Environ. Au* **2022**, *2*, 549.
[47] A. Hakim, M. Kobayashi, *J. Polym. Environ.* **2021**, *29*, 1921.
[48] D. Takács, T. Szabó, A. Jamnik, M. Tomšič, I. Szilágyi, *Langmuir* **2023**, *39*, 12835.
[49] G. V. Quincke, *Ann. Phys. (Berlin)* **1861**, *189*, 513.
[50] Z. Adamczyk, M. Zembala, A. Michna, *J. Colloid Interface Sci.* **2006**, *303*, 353.
[51] A. E. Childress, M. Elimelech, *Environ. Sci. Technol.* **2000**, *34*, 3710.
[52] C. Werner, R. Zimmermann, T. Kratzmüller, *Colloids Surf. A.* **2001**, *192*, 205.
[53] Z. Adamczyk, K. Sadlej, E. Wajnryb, M. Nattich, M. L. Ekiel-Jezewska, J. Bławzdziewicz, *Adv. Colloid Interface Sci.* **2010**, *153*, 1.
[54] Z. Adamczyk, M. Zaucha, M. Zembala, *Langmuir* **2010**, *26*, 9368.
[55] J. F. L. Duval, R. Zimmermann, A. L. Cordeiro, N. Rein, C. Werner, *Langmuir* **2009**, *25*, 10691.
[56] J. F. Duval, D. Küttner, C. Werner, R. Zimmermann, *Langmuir* **2011**, *27*, 10739.
[57] R. Schweiss, P. B. Welzel, C. Werner, W. Knoll, *Langmuir* **2001**, *17*, 4304.
[58] C. Werner, H. Körber, R. Zimmermann, S. Dukhin, H. J. Jacobasch, *J. Colloid Interface Sci.* **1998**, *208*, 329.
[59] M. Zembala, Z. Adamczyk, *Langmuir* **2000**, *16*, 1593.
[60] R. Zimmermann, S. Dukhin, C. Werner, *J. Phys. Chem. B.* **2001**, *105*, 8544.
[61] R. Zimmermann, U. Freudenberg, R. Schweiß, D. Küttner, C. Werner, *Curr. Opin. Colloid Interface Sci.* **2010**, *15*, 196.
[62] R. Akhbarizadeh, S. Dobaradaran, M. A. Torkmahalleh, R. Saeedi, R. Aibaghi, F. F. Ghasemi, *Environ. Res.* **2021**, *192*, 110339.
[63] J. Brehm, M. V. Wilde, L. Reiche, L. C. Leitner, B. Petran, M. Meinhart, S. Wieland, S. Ritschar, M. Schott, J. P. Boos, S. Frei, H. Kress, J. Senker, A. Greiner, T. Fröhlich, C. Laforsch, *J. Hazard. Mater.* **2022**, *437*, 129351.
[64] C. F. Araujo, M. M. Nolasco, A. M. P. Ribeiro, P. J. A. Ribeiro-Claro, *Water Res.* **2018**, *142*, 426.
[65] E. Fries, J. H. Dekiff, J. Willmeyer, M. T. Nuelle, M. Ebert, D. Remy, *Environ. Sci.: Process. Impacts.* **2013**, *15*, 1949.
[66] N. Meides, T. Menzel, B. Poetzschner, M. G. J. Löder, U. Mansfeld, P. Strohriegl, V. Altstaedt, J. Senker, *Environ. Sci. Technol.* **2021**, *55*, 7930.
[67] J. Wagner, Z.-M. Wang, S. Ghosal, C. Rochman, M. Gassel, S. Wall, *Anal. Methods* **2017**, *9*, 1479.
[68] A. Mauel, B. Pötzschner, N. Meides, R. Siegel, P. Strohriegl, J. Senker, *RSC Adv.* **2022**, *12*, 10875.
[69] J. Schmidt, M. Haave, J. Underhaug, W. Wang, *Microplast. Nanoplast.* **2024**, *4*, 1.
[70] D. W. Fuerstenau, *PhD Thesis*, Massachusetts Institute of Technology **1953**.
[71] V. Pravdic, *Croat. Chem. Acta* **1958**, *30*, 113.
[72] M. A. Hubbe, F. Wang, *Paper Technol.* **2004**, *45*, 27.
[73] O. El-Gholabzouri, M. A. Cabrerizo, R. Hidalgo-Álvarez, *J. Colloid Interface Sci.* **1998**, *199*, 38.
[74] O. El-Gholabzouri, M. A. Cabrerizo, R. Hidalgo-Álvarez, *Colloids Surf. A.* **1999**, *159*, 449.
[75] R. Hidalgo-Álvarez, F. J. D. L Nieves, G. Pardo, *J. Colloid Interface Sci.* **1985**, *107*, 295.
[76] E. Rodier, J. Dodds, *Part. Part. Syst. Charact.* **1995**, *12*, 198.
[77] A. Drechsler, A. Caspari, A. Synytska, *Surf. Interface Anal.* **2020**, *52*, 991.
[78] E. Walker, P. W. J. Glover, *Transp. Porous Media* **2018**, *121*, 183.
[79] D. Jougnot, N. Linde, A. Revil, C. Doussan, *Vadose Zone J.* **2012**, *11*, 1.
[80] Z. Li, Y. Liu, D. Wang, P. Wang, R. Xu, D. Xie, *Eur. J. Soil Sci.* **2019**, *70*, 1063.
[81] C. M. Mboh, J. A. Huisman, E. Zimmermann, H. Vereecken, *Vadose Zone J.* **2012**, *11*, 1.
[82] N. Meides, A. Mauel, T. Menzel, V. Altstädt, H. Ruckdäschel, J. Senker, P. Strohriegl, *Microplast Nanoplast.* **2022**, *2*, 1.
[83] J. N. Möller, I. Heisel, A. Satzger, E. C. Vizsolyi, S. D. J. Oster, S. Agarwal, C. Laforsch, M. G. J. Löder, *Environ. Toxicol. Chem.* **2022**, *41*, 844.
[84] A. F. R. M. Ramsperger, A. C. Stellwag, A. Caspari, A. Fery, T. Lueders, H. Kress, M. G. J. Löder, C. Laforsch, *Water (Basel).* **2020**, *12*, 3216.
[85] B. Trotter, M. V. Wilde, J. Brehm, E. Dafni, A. Aliu, G. J. Arnold, T. Fröhlich, C. Laforsch, *Sci. Total Environ.* **2021**, *795*, 148822.
[86] M. Völkl, V. Jérôme, A. Weig, J. Jasinski, N. Meides, P. Strohriegl, T. Scheibel, R. Freitag, *J. Hazard. Mater.* **2022**, *435*, 128955.
[87] M. Minor, A. J. van der Linde, J. Lyklema, *J. Colloid Interface Sci.* **1998**, *203*, 177.
[88] M. Minor, A. J. van der Linde, H. P. van Leeuwen, J. Lyklema, *Colloids Surf. A.* **1998**, *142*, 165.
[89] N. Spanos, A. Tsevis, P. G. Koutsoukos, M. Marcel, A. J. van der Linde, J. Lyklema, *Colloids Surf. A.* **1998**, *141*, 101.
[90] H. J. Jacobasch, G. Bauböck, J. Schurz, *Colloid Polym. Sci.* **1985**, *263*, 3.
[91] H.-J. Jacobasch, J. Schurz, *Prog. Colloid Polym. Sci.* **1988**, *77*, 40.
[92] S. Laha, M. Roy, S. Chakraborty, *Langmuir* **2024**, *40*, 12878.
[93] O. Duliu, *Earth-Sci. Rev.* **1999**, *48*, 265.
[94] J. K. Jasti, G. Jesion, L. Feldkamp, *SPE Form. Eval.* **1993**, *8*, 189.
[95] H. Ohshima, *Electrical Phenomena at Interfaces and Biointerfaces: Fundamentals and Applications in Nano-, Bio-, and Environmental Sciences*, Wiley, New York / Chichester, UK **2012**.
[96] H. C. Li, P. L. De Bruyn, *Surf. Sci.* **1966**, *5*, 203.
[97] S. Chakraborty, *Phys. Rev. Lett.* **2008**, *100*, 097801.
[98] C. Zhao, C. Yang, *Colloids Surf. A.* **2011**, *386*, 191.
[99] H. Ohshima, T. W. Healy, L. R. White, *J. Colloid Interface Sci.* **1982**, *90*, 17.
[100] S. H. Behrens, M. Borkovec, P. Schurtenberger, *Langmuir* **1998**, *14*, 1951.
[101] R. Ruiz, C. Ràfols, M. Rosés, E. Bosch, *J. Pharm. Sci.* **2003**, *92*, 1473.
[102] A. Homola, R. O. James, *J. Colloid Interface Sci.* **1977**, *59*, 123.
[103] K. G. Marinova, R. G. Alargova, N. D. Denkov, O. D. Velev, D. N. Petsev, I. B. Ivanov, R. P. Borwankar, *Langmuir* **1996**, *12*, 2045.
[104] V. Tandon, S. K. Bhagavatula, W. C. Nelson, B. J. Kirby, *Electrophoresis* **2008**, *29*, 1092.
[105] L. P. Voegtli, C. F. Zukoski, *J. Colloid Interface Sci.* **1991**, *141*, 92.
[106] M. Elimelech, W. H. Chen, J. J. Waypa, *Desalination* **1994**, *95*, 269.
[107] H. Müller, W. Leube, K. Tauer, S. Förster, M. Antonietti, *Macromolecules* **1997**, *30*, 2288.
[108] S. Lu, K. Zhu, W. Song, G. Song, D. Chen, T. Hayat, N. S. Alharbi, C. Chen, Y. Sun, *Sci. Total Environ.* **2018**, *630*, 951.
[109] Q. M.égier du Sorbier, A. Aimable, C. Pagnoux, *J. Colloid Interface Sci.* **2015**, *448*, 306.
[110] Y. Utashiro, M. Takiguchi, M. Satoh, *Colloid Polym. Sci.* **2017**, *295*, 45.
[111] Y.-H. M. Chan, R. Schweiss, C. Werner, M. Grunze, *Langmuir* **2003**, *19*, 7380.

[112] J. K. Beattie, *Lab. Chip* **2006**, *6*, 1409.
[113] A. M. Pineda-Reyes, M. Hernández Delgado, M. D. L. L. Zambrano-Zaragoza, G. Leyva-Gómez, N. Mendoza-Muñoz, D. Quintanar-Guerrero, *RSC Adv.* **2021**, *11*, 2226.
[114] J. F. Duval, *J. Phys. Chem. A.* **2009**, *113*, 2275.
[115] A. Michna, *Adv. Colloid Interface Sci.* **2017**, *250*, 95.
[116] C. J. McColley, J. A. Nason, B. J. Harper, S. L. Harper, *Microplast Nanoplast.* **2023**, *3*, 10.
[117] M. Wisniewska, I. Ostolska, K. Szewczuk-Karpisz, S. Chibowski, K. Terpiłowski, V. M. Gun'ko, V. I. Zarko, *J. Nanopart. Res.* **2015**, *17*, 12.
[118] J. Xu, M. Li, Y. Zhao, Q. Lu, *Colloids Surf. A.* **2007**, *302*, 136.
[119] P. Beneš, M. Paulenová, *Z. Polym.* **1973**, *251*, 766.
[120] V. Kuznetsov, G. Papastavrou, *J. Phys. Chem. C.* **2014**, *118*, 2673.
[121] C. C. Price, R. W. Kell, E. Krebs, *J. Am. Chem. Soc.* **1942**, *64*, 1103.
[122] J. A. Mielczarski, Y. L. Jeyachandran, E. Mielczarski, B. Rai, *J. Colloid Interface Sci.* **2011**, *362*, 532.
[123] A. J. Everett, G. J. Minkoff, *Trans. Faraday Soc.* **1953**, *49*, 410.
[124] J. P. Guthrie, J. Cossar, A. Klym, *J. Am. Chem. Soc.* **1982**, *104*, 895.
[125] W. Li, B. Zu, Q. Yang, J. Guo, J. Li, *RSC Adv.* **2023**, *13*, 15566.
[126] M. B. Engelhardt, P. Markus, N. Helfricht, G. Papastavrou, *J. Colloid Interface Sci.* **2025**, *686*, 852.
[127] J. Schindelin, I. Arganda-Carreras, E. Frise, V. Kaynig, M. Longair, T. Pietzsch, S. Preibisch, C. Rueden, S. Saalfeld, B. Schmid, J. Y. Tinevez, D. J. White, V. Hartenstein, K. Eliceiri, P. Tomancak, A. Cardona, *Nat. Methods* **2012**, *9*, 676.

Manuscript received: July 30, 2025
Revised manuscript received: August 23, 2025
Version of record online: September 22, 2025